# Supporting Information

# Heterojunction-Redox Catalysts of $Fe_xCo_yMg_{10}CaO$ for High-Temperature $CO_2$ Capture and In-situ Conversion

Bin Shao [a], Guihua Hu[b], Khalil A. M. Alkebsi[b], Guanghua Ye[c], Xiaoqing Lin [a], Wenli Du [b], Jun Hu [a*], Meihong Wang [d*], Honglai Liu [a], Feng Qian [b]

[a.] School of Chemistry and Molecular Engineering, East China University of Science and Technology, 130 Meilong Road, Shanghai 200237, China.

[b.] Key Laboratory of Advanced Control and Optimization for Chemical Processes of Ministry of Education, East China University of Science and Technology, 130 Meilong Road, Shanghai 200237, China

[c.] State Key Laboratory of Chemical Engineering, East China University of Science and Technology, 130 Meilong Road, Shanghai 200237, China.

[d.] Department of Chemical and Biological Engineering, The University of Sheffield, Sheffield S1 3JD, United Kingdom.

## Adsorption kinetics

To investigate kinetics of adsorption of $CO_2$ on synthesized $\mathbf{Fe_xCo_yMg_{10}CaO}$ and **CaO**, the following the pseudo-second order model was used.[1]

$$q_t = \frac{kq_e^2 t}{1 + kq_e t} \quad (1)$$

where,

$k$ = reaction rate constant of the pseudo-second order model in g $mmol^{-1}$ $min^{-1}$.

$q_e$ = amount adsorbed at equilibrium in mmol $g^{-1}$

$q_t$ = amount adsorbed (in mmol $g^{-1}$) at time t in min

## Computer modeling and simulation study

To study the scalability of proposed novel technology at the commercial scale, we carried out a computer modeling and simulation study through gPROMS ModelBuilder®(V4.0). As we mentioned in the manuscript, the energy consumed by the high-temperature thermal cracking furnace in the ethylene industry is usually provided by the combustion of natural gas. It is reported that manufacturing one ton of ethylene produces between 1 to 2 tons of $CO_2$. A 100,000 t/yr ethylene plant, corresponding to 100,000 t/yr $CO_2$ emission, was selected as the $CO_2$ resource to study the scalability of this integrated CaL/RWGS process.

The simulation equations of $CO_2$ adsorption and conversion, the simulation parameters of each process and the available fundamental experimental data are as following:

### (1) Models and boundary conditions of the $CO_2$ adsorption process

Mass balance

$$\varepsilon \frac{\partial C_i}{\partial t} + (1-\varepsilon)\rho \frac{\partial q_i}{\partial t} = \varepsilon \frac{\partial}{\partial z}\left( D_{ax} \frac{\partial C_i}{\partial z} \right) - \frac{\partial (uC_i)}{\partial z} \quad (2)$$

$$C_i = C_{i,0} \;\; at\; t = 0, 0 \le z \le L$$

$$\frac{\partial C_i}{\partial z} = 0 \;\; at\; z = L, t > 0$$

$$D_{ax} \frac{\partial C_i}{\partial z} = u(C_i - C_{i,0}) \;\; at\; z = 0, t > 0$$

Adsorption isotherm

$$q = q_{sat} \frac{bP_{CO_2}}{1 + bP_{CO_2}} \quad (3)$$

Energy balance

$$\varepsilon C_t C_{p,v} \frac{\partial T}{\partial t} + (1-\varepsilon)\rho C_{ps} \frac{\partial T}{\partial t} = -uC_t C_{p,p} \frac{\partial T}{\partial z} + (1-\varepsilon)\rho(-\Delta H)\frac{\partial q_i}{\partial t} \quad (4)$$

$$T = T_0 \;\; at\; t = 0, 0 \le z \le L$$

$$\frac{\partial T}{\partial z} = 0 \;\; at\; z = L, t > 0$$

$$T = T_0 \;\; at\; z = 0, t > 0$$

Simulation parameters of the $CO_2$ adsorption process

| | |
|---|---|
| Inlet flue gas temperature | 923 K |
| Pressure at the fixed-bed column | 1 atm |
| $CO_2$ molar concentration in inlet flue gas | 1.32 mol $m^{-3}$ |

| | |
|---|---|
| adsorbent density | 1600 kg $m^{-3}$ |
| porosity of bed | 0.35 |
| Flue gas flow rate | 10 m $s^{-1}$ |
| bed length | 10 m |
| Reactor diameter | 2.5 m |
| Molar heat capacity at constant volume | 20.7 J $mol^{-1}$ $K^{-1}$ |
| Molar heat capacity at constant pressure | 29.1 J $mol^{-1}$ $K^{-1}$ |
| Heat capacity of adsorbent | 1000 J $kg^{-1}$ $K^{-1}$ |
| axial back-mixing | 1e$^{-5}$ $m^2$ $s^{-1}$ |
| Total concentration of flue gas | 13.2 mol $m^{-3}$ |

**(2) Models and boundary conditions of the conversion process**

Mass balance

$$\varepsilon \frac{\partial C_{\mathrm{H}_2}}{\partial t} = \varepsilon \frac{\partial}{\partial z}\left( D_{ax} \frac{\partial C_{H_2}}{\partial z} \right) - \frac{\partial \left( u C_{H_2} \right)}{\partial z} - \left(1-\varepsilon\right)\rho k \frac{q}{q_{sat}} \frac{C_{\mathrm{H}_2}}{C_{\mathrm{H}_2,in}} \tag{5}$$

$$\frac{\partial q}{\partial t} = k \frac{q}{q_{sat}} \frac{C_{\mathrm{H}_2}}{C_{\mathrm{H}_2,b}} \tag{6}$$

$$C_{CO} = C_{CO,in} + C_{H_2,in} - C_{H_2} \tag{7}$$

$$C_{H_2O} = C_{H_2O,in} + C_{H_2,in} - C_{H_2} \tag{8}$$

Energy balance

$$\varepsilon C_t C_{p,v} \frac{\partial T}{\partial t} + (1-\varepsilon)\rho C_{ps} \frac{\partial T}{\partial t} = -uC_t C_{p,p} \frac{\partial T}{\partial z} + (1-\varepsilon)\rho(-\Delta H)\frac{\partial q_i}{\partial t} \quad (9)$$

$$C_{H_2} = 0 \;\; at\; t = 0, 0 \le z \le L$$

$$\frac{\partial C_{H_2}}{\partial z} = 0 \;\; at\; z = L, t > 0$$

$$D_{ax} \frac{\partial C_{H_2}}{\partial z} = u(C_{H_2} - C_{H_2,0}) \;\; at\; z = 0, t > 0 \quad (10)$$

$$T = T_0 \;\; at\; t = 0, 0 \le z \le L$$

$$\frac{\partial T}{\partial z} = 0 \;\; at\; z = L, t > 0$$

$$T = T_0 \;\; at\; z = 0, t > 0$$

Simulation parameters of the conversion process

| | |
|---|---|
| $H_2$ inlet temperature | 923 K |
| Pressure at the fixed-bed column | 1 atm |
| $H_2$ molar concentration | 13.2 mol $m^{-3}$ |
| adsorbent density | 1600 kg $m^{-3}$ |
| porosity of bed | 0.35 |
| $H_2$ flow rate | 1 m $s^{-1}$ |
| bed length | 10 m |
| Reactor diameter | 2.5 m |
| Molar heat capacity at constant volume | 20.7 J $mol^{-1}$ $K^{-1}$ |
| Molar heat capacity at constant pressure | 29.1 J $mol^{-1}$ $K^{-1}$ |
| Heat capacity of adsorbent | 1000 J $kg^{-1}$ $K^{-1}$ |

| | |
|---|---|
| axial back-mixing | 1e-5 $m^2 s^{-1}$ |
| Total concentration of flue gas | 13.2 mol $m^{-3}$ |

Thermodynamic and kinetic experimental data for $CO_2$ adsorption and conversion reaction.

| Adsorption process | |
|---|---|
| $q_{sat}$ (mol $kg^{-1}$) | 10.21 |
| $b_0$ ($atm^{-1}$) | 0.27 |
| $\Delta_r H$m (kJ $mol^{-1}$) | -177 |
| **Conversion process** | |
| $k$ (mol $min^{-1}$ $kg^{-1}$) | 0.08 |
| $\Delta_r H$m (kJ $mol^{-1}$) | 213 |
| $E$a (kJ $mol^{-1}$) | 52.97 |

To simulate the ethylene plant with an annual production of 100,000 tons, corresponding to 100,000 tons $CO_2$/yr emission, the column of the integrated CaL/RWGS process is set as 2,500 mm ×10,000 mm, and 50 t $Fe_5Co_5Mg_{10}CaO$ (with the $CO_2$ adsorption capacity of 9 mol $kg^{-1}$) are used to operate the integrated CaL/RWGS process. As shown in **Fig. S15a**, when the flow rate of the flue gas (10 vol. % $CO_2$) is set as 10 m $s^{-1}$, the breakthrough time is calculated as 7200 s, corresponding to the total throughput of 138 t flue gas and 19.5 t $CO_2$ (the capture efficiency of about 95%). Meanwhile, when the temperature of the inlet flue gas is set at 650℃, the temperature profile reveals an increase of the local temperature of the reactor to the maximum of 884℃ due to the exothermic adsorption process (**Fig. S15c**). With the heat carried out by the flow gas, the overall temperature of the column is relatively stable during the adsorption process.

After the breakthrough of the CaL process, the feed gas is switched to pure $H_2$ with the flow rate of 1 m $s^{-1}$ and the temperature of 650 ℃. As the fast reaction rate of RWGS

conversion (reaction rate constant $k = 0.08$ mol $min^{-1}$ $kg^{-1}$), $H_2$ reacts with the adsorbed $CO_2$ to produce CO immediately. During the initial 2400 seconds, the produced CO holds a stable concentration of 13.2 mol $m^{-3}$ in the outlet; when the reaction continues, the gradually decreased $CO_2$ concentration leads to the incomplete reaction of $H_2$. Overall, the $CO_2$ conversion reaches as high as 90% with the CO selectivity of 100% at 7200 s (**Fig. S15b**). During the conversion process, we can control the molar ratio of CO to $H_2$ in the outlet by stopping the reaction at an appropriate time and provide syngas for the further downstream Fischer-Tropsch synthesis.

As the RWGS reaction is endothermic, an extra heat needs to be supplied to maintain a relatively constant temperature during the conversion process. Particularly, when the heat released in the first adsorption stage is reused and an extra heat of 36 kJ $mol^{-1}(CO_2)$ is input in in this conversion stage, the temperature profile shows a small temperature drops of about 20 ℃ in the middle of the column (**Fig. S15d**). Overall, the temperature holds at 650℃ throughout the conversion process.

The $CO_2$ capture capacity and conversion efficiency holds almost constant after 10 cycles (**Fig.S16**). Therefore, the simulation study showed a stable performance of the simultaneous $CO_2$ capture and in-situ conversion at the commercial scale.

## Economic evaluation

To capture around 100,000 t/yr pure $CO_2$ emission in an ethylene plant, the flow rate of the flue gas (10 vol% $CO_2$) is set as $8.4 \times 10^4$ kg/h with assuming the yearly operating time as 8000 h/yr. Based on the temperature profile of the thermal cracking furnace in ethylene plant, the flue gas with the temperature of 650 ℃ is directed into the column filled with the bifunctional adsorbent/catalyst of **$Fe_5Co_5Mg_{10}CaO$.**

(1) $CO_2$ adsorption at 650 $^oC$ and at normal pressure through CaL, with the $CO_2$ capture efficiency of 95%, the treated gas is released.

(2) $CO_2$ conversion at the same temperature of 650 °C and at atmospheric pressure. By switching the flue gas into pure $H_2$, CO is produced through RWGS reaction. The syngas of CO and $H_2$ with proper molar ratio is produced in the outlet for the downstream Fischer-Tropsch synthesis. Without any additional desorption process, **$Fe_5Co_5Mg_{10}CaO$** is regenerated for the next cycle of $CO_2$ adsorption and conversion.

The main energy consumption during this integrated CaL/RWGS process (Fig. S17 in revised SI) includes electric work of the blower for the gas transport, the heat for heating $H_2$ from 25℃ to 650℃, and the heat for maintaining the conversion temperature at 650 °C due to the endothermic RWGS reaction.

The electric work of the blower $W_b$ is calculated by

$$W_b = Q \times p \times t / \eta_0 \quad (11)$$

where $Q$ ($m^3$/h) is the flow rate, $p$ (Pa) is the gas pressure, $t$ is working time (h), $\eta_0$ is the efficiency of blower, usually, $\eta_0$=0.75[2]. The electric work of gas blower includes three parts, for flue gas, $H_2$ and the reuse of flue gas.

The heat $Q_1$ for heating $H_2$ from 25 °C to 650 °C is calculated by

$$Q_1 = n \times C_p \times (T_2 - T_1) \quad (12)$$

where $n$ (*mol*) is amount of $H_2$ necessary for the conversion, $C_p$ (J/mol K) is the average heat capacity of $H_2$, $T_1$ and $T_2$ are the initial temperature (298 K) and final temperature (923 K) of $H_2$. $Q_1$ is provided by the combustion of natural gas, therefore, the total amount of natural gas ($n_{NG}$) needs

$$n_{NG} = Q_1 / (Q_{NG} \times \eta_1 \times 22.4) \quad (13)$$

where $Q_{NG}$ (kJ/$L^3$ (STP)) is the heat value of the natural gas, with the value of 34.3 kJ/$L^3$ (STP)[3], $\eta_1$ is heating efficiency, usually, $\eta_1$ = 0.75 [4].

The heat $Q_2$ for maintaining the conversion temperature at 650 °C is calculated by

$$Q_2 = n_{CO2} \times (\Delta H_{ad} + \Delta H_{RWGS}) / \eta_2 \quad (14)$$

where $n_{CO2}$ ($mol$) is amount of $CO_2$, $\Delta H_{ad}$ is the reaction enthalpy of the exothermic CaL, $\Delta H_{RGWS}$ is the reaction enthalpy of the endothermic RGWS reaction, $\eta_2$ is the efficiency of the heat exchange, usually $\eta_2$=0.8. $Q_2$ is provided by the electricity, therefore, the total amount of electricity, $W_h$, is

$$W_h = Q_2 / \eta_3 \quad (15)$$

where $\eta_3$ is the efficiency of the heating, usually $\eta_3$=0.95.

The flue gas is simplified as 10 vol% $CO_2$ + 90 vol% $N_2$. Based on the scale-up experimental and simulation results, the $CO_2$ capture efficiency is set as 95%, and the conversion efficiency is set as 85% (5% decreases for the unforeseen circumstances), with the CO selectivity of 100%. The molar ratio of $H_2$ to converted $CO_2$ is set as 3:1. All the material flow and consumption (per hour) during this integrated CaL/RWGS process for the treatment of 672,000 t/yr (84t/h) flue gas are calculated and listed in **Table S10** and **Table S11**.

The economic analysis of the integrated CaL/RWGS process is listed in Table 2. The operation costs are mainly dominated by materials of $H_2$ ($12.5 million/yr) and **$Fe_5Co_5Mg_{10}CaO$** ($0.58 million/yr), electricity for blowers and heating ($2.16 million/yr), and natural gas for heating ($1.72 million/yr). Among them, $H_2$ is the cost-determining factor. In fact, $H_2$ is a by-product of the ethylene plant, accounting for about 1% of the total output, then the cost of 2000 t/yr $H_2$ can be saved.[5] As a result, the operation cost for the integrated CaL/RWGS process is about $165/t $CO_2$, much lower than the reported operation cost of separated RWGS process of $323/t $CO_2$ [6]. In addition, the operation cost of the separated CaL process is $72/t $CO_2$ in the literature[7]. It is worth to mention, after the CaL process, $CO_2$ needs to be compressed and

transported, which accounts for at least \$20/t $CO_2$ for the transport, let alone the huge capital costs of trunk pipeline network and collecting system. [8] If we simply combine two reported separated CaL and RWGS process together, the operation cost will account for at least \$393/t $CO_2$. Therefore, based on the novel adsorbent and catalyst of **$Fe_5Co_5Mg_{10}CaO$,** the integrated CaL/RWGS process can be applied to the ethylene plants more cost-effectively. About 67% of unreacted $H_2$ remains in the outlet, together with converted CO, they form a syngas (the molar ratio of $H_2$:CO=2:1) for the downstream Fischer-Tropsch synthesis, which will account for \$9.38 million/yr, almost covering the total cost of integrated CaL/RWGS process. Moreover, with $CO_2$ capture and conversion taking place in the same column, it will save a great deal of capital costs.

Overall, energy recovery directly using high-temperature flue gas to realize the $CO_2$ capture and to provide the required energy for simultaneous conversion, the integrated CaL/RWGS technology provides a promising way for the green manufacturing in chemical industries.

## Figures and Tables

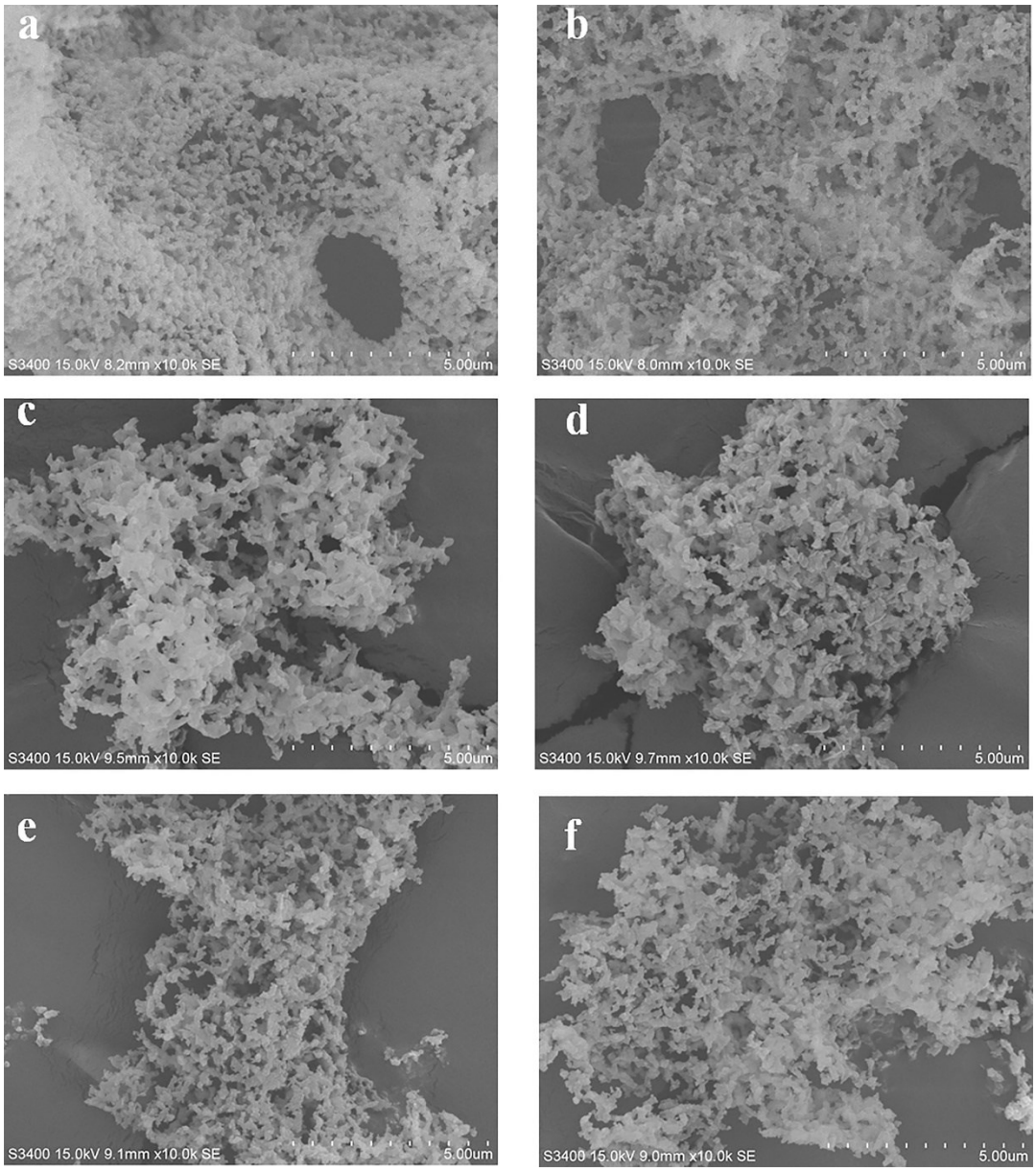


**Fig. S1** SEM images of (a) **$Fe_{10}Mg_{10}CaO$**, (b) **$Co_{10}Mg_{10}CaO$**, (c) **$Fe_{3.3}Co_{6.7}Mg_{10}CaO$** (d) **$Fe_{6.7}Co_{3.3}Mg_{10}CaO$** (e) **$Fe_{7.5}Co_{2.5}Mg_{10}CaO$** and (f) **$Fe_8Co_2Mg_{10}CaO$.**

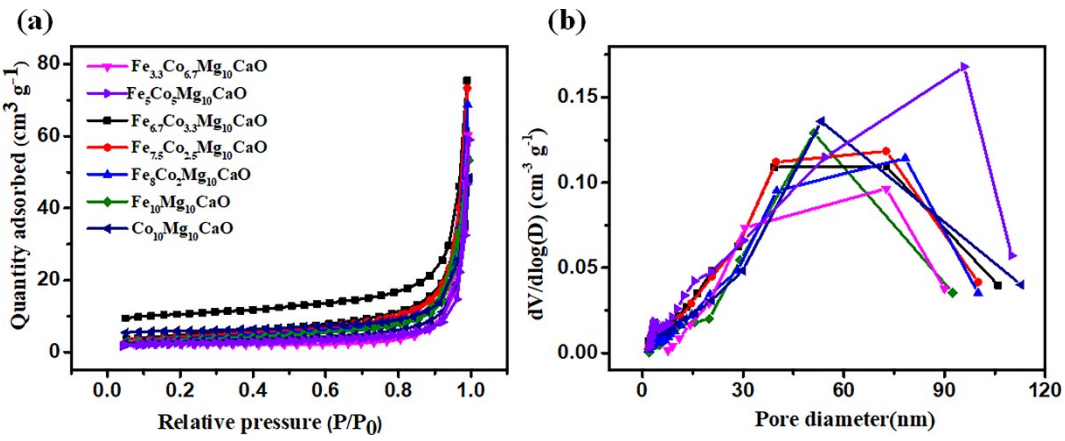


**Fig. S2** (a) $N_2$ adsorption-desorption isotherms and (b) pore size distribution of $\mathbf{Fe_xCo_yMg_{10}CaO}$.

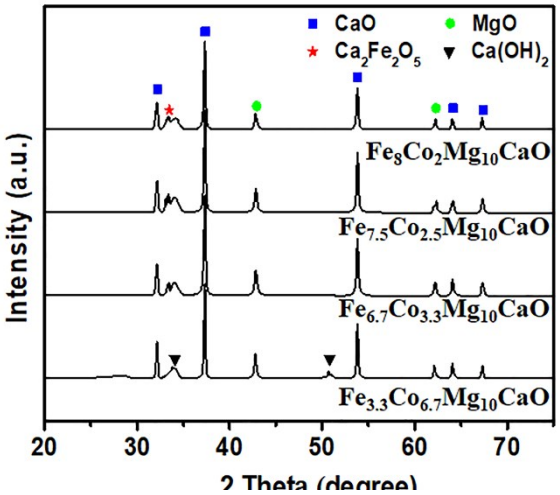


**Fig. S3** The XRD patterns of $\mathbf{Fe_xCo_yMg_{10}CaO}$ (Fe/Co=0.5, 2, 3, 4).

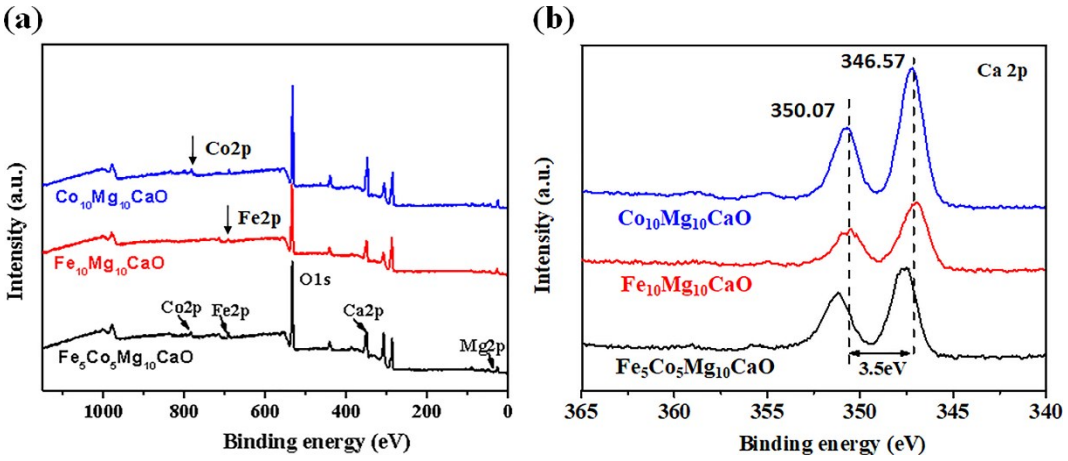


**Fig. S4** The XPS spectra of (a) the elemental survey scan of Ca, Mg, Fe, Co, respectively and (b) Ca2p. XPS spectra of **$Fe_xCo_yMg_{10}CaOs$**.

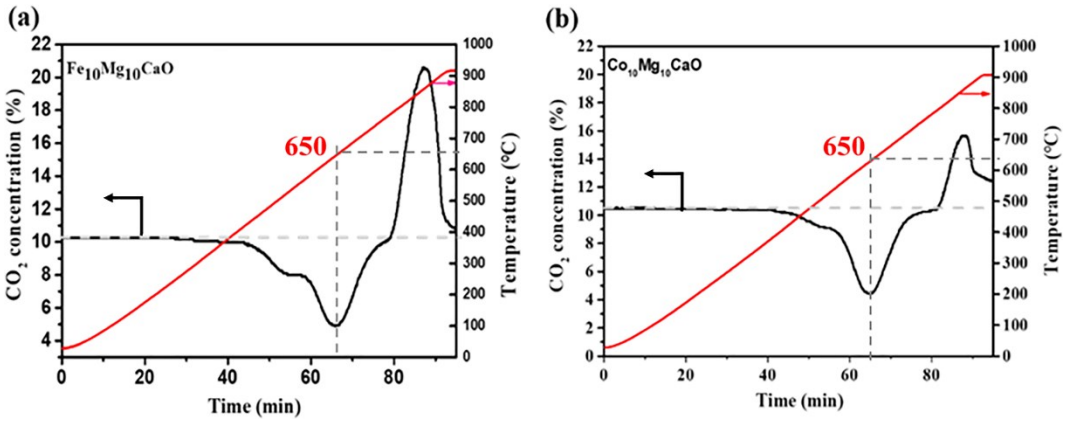


**Fig. S5** Dynamic $CO_2$ uptakes from the simulated flue gas (the molar ratio of $CO_2$:$N_2$=1:9) in the temperature range of 30 °C to 900 °C on(a) **$Fe_{10}Mg_{10}CaO$** and (b) **$Co_{10}Mg_{10}CaO$**.

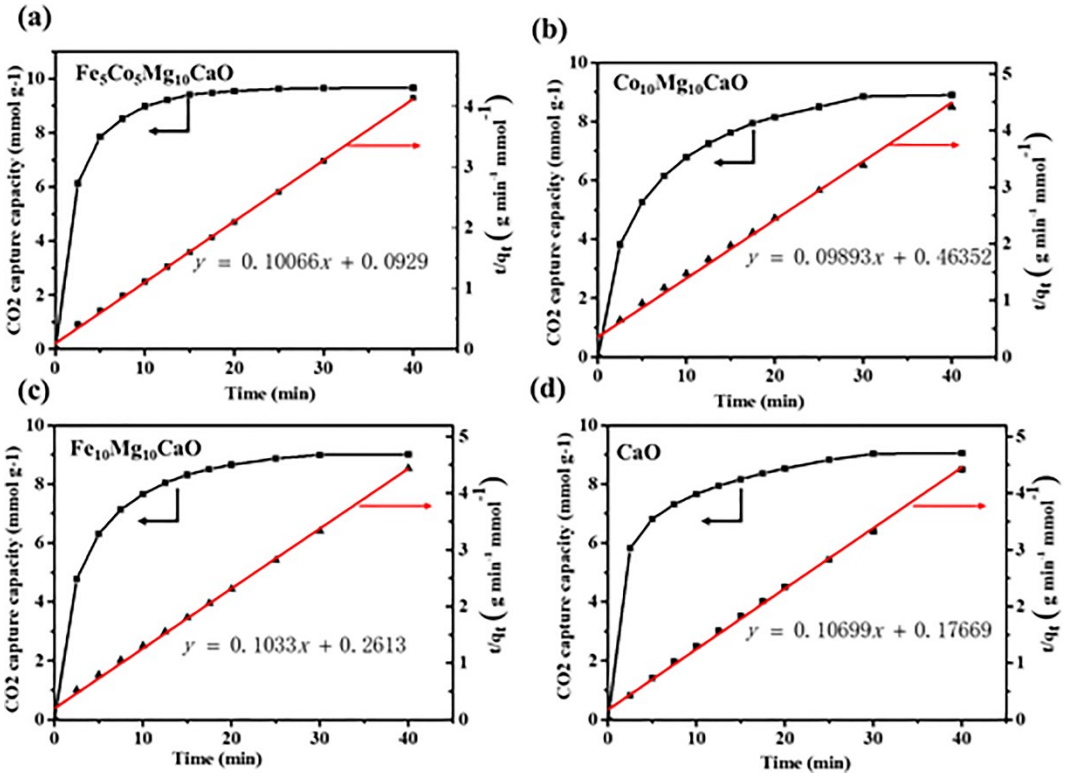


**Fig. S6** adsorption kinetic curves and pseudo-second-order kinetic fitting curves of **$Fe_xCo_yMg_{10}CaO$** and **CaO** at 650 ℃.

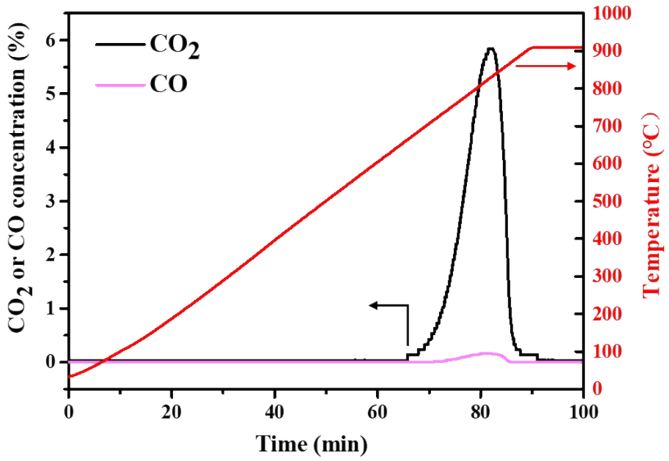


**Fig. S7** Dynamic $CO_2$ desorption performance on **$Fe_5Co_5Mg_{10}CaO$ purged by** pure $N_2$ in the temperature range of 30-900℃.

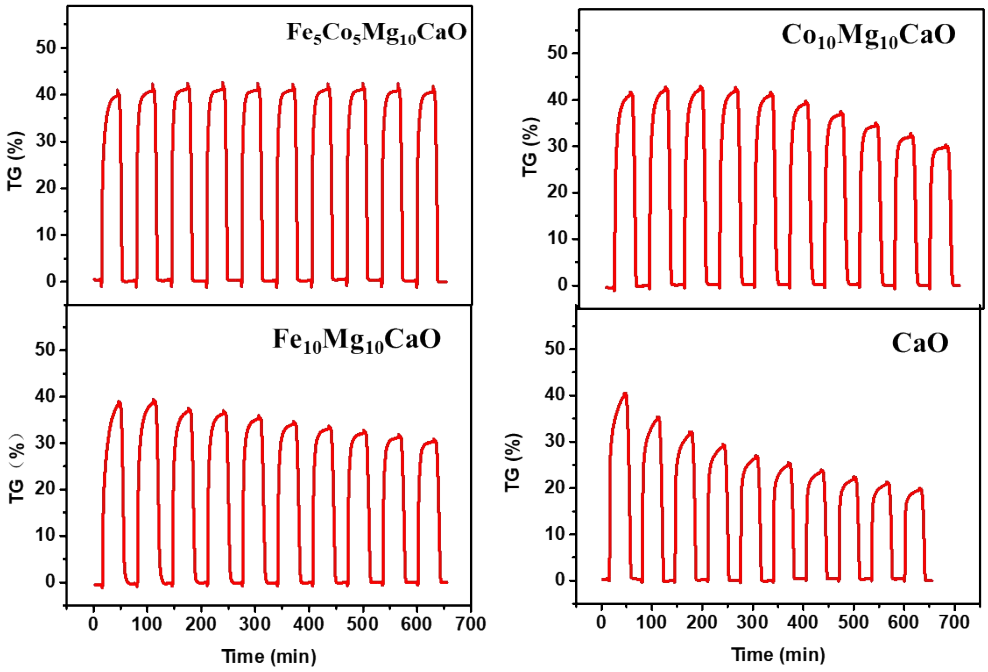


**Fig. S8** 10 cycles $CO_2$ adsorption-desorption stability on **$Fe_xCo_yMg_{10}CaO$** and **CaO** at 650℃.

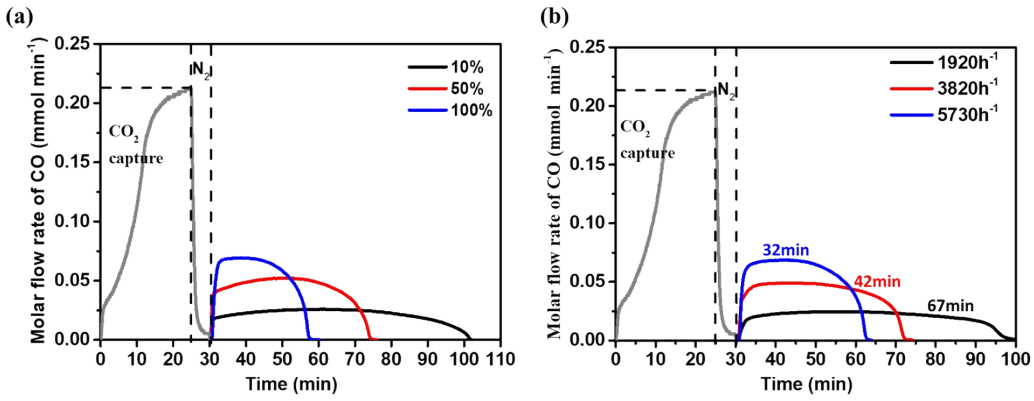


**Fig. S9** $CO_2$ adsorption and CO production under the inlet gas with (a) various $H_2$ contents and (b) various $H_2$ GHSV on **$Fe_5Co_5Mg_{10}CaO$** at 650 ℃.

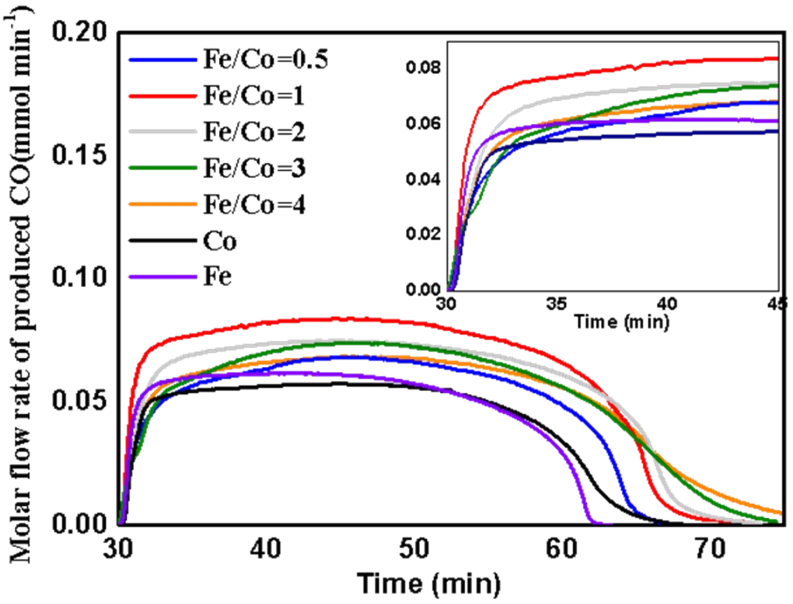


**Fig. S10** Molar flow rate of CO produced on $\mathbf{Fe_xCo_yMg_{10}CaO}$ (with different Fe/Co mass ratios) under the optimal conversion conditions (at 650 ℃ and the flow rate $H_2$ of 50mL/min).

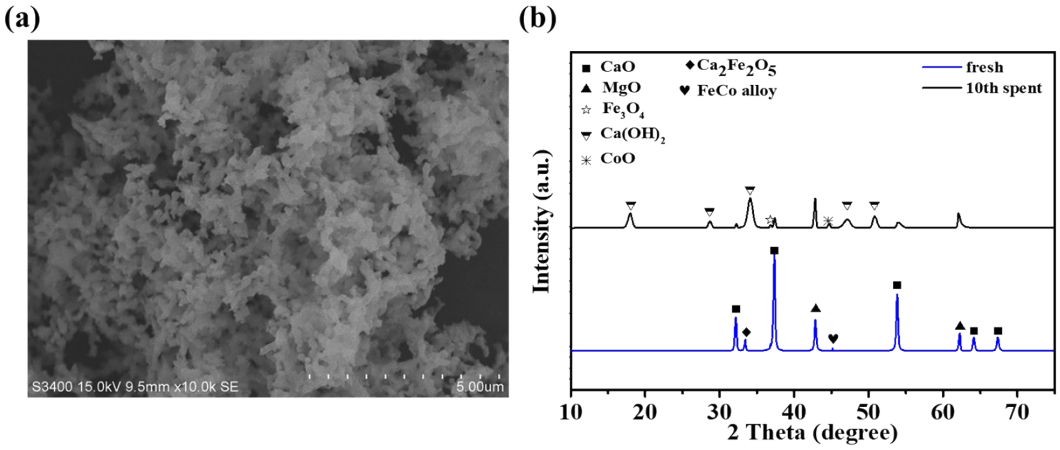


**Fig. S11 (**a) SEM image and (b) XRD patterns of $\mathbf{Fe_5Co_5Mg_{10}CaO}$ after 10 cyclic integrated $CO_2$ capture and in-situ conversion.

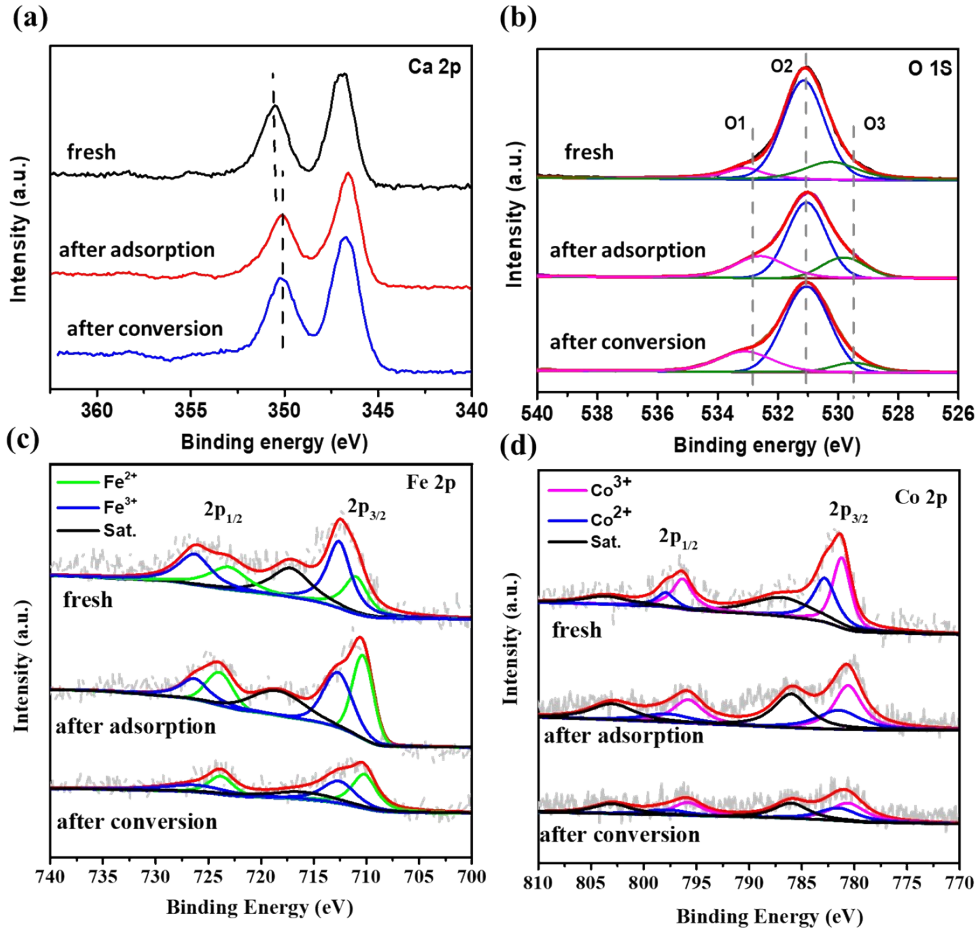


**Fig. S12** the high-resolution XPS spectra of (a) Ca 2p, (b) O1s, (c) Fe 2p, and (d) Co 2p of **$Fe_5Co_5Mg_{10}CaO$** at different stages of fresh, after adsorption and after conversion.

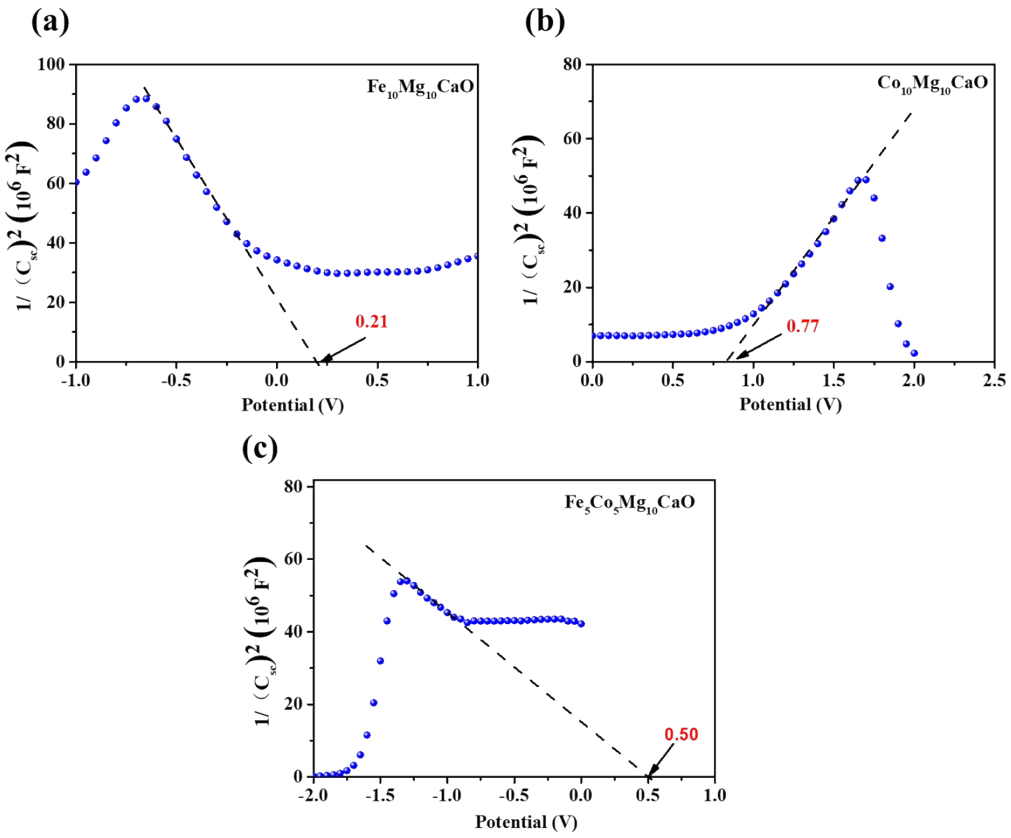


**Fig. S13** Mott-Schottky plots of (a) **$Co_{10}Mg_{10}CaO$**; (b) **$Fe_{10}Mg_{10}CaO$**, and (c) **$Fe_5Co_5Mg_{10}CaO$.**

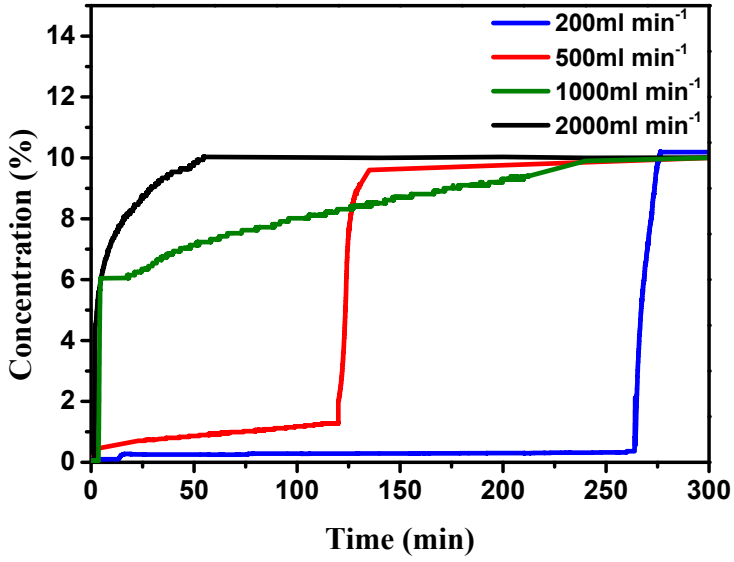


**Fig. S14** The $CO_2$ adsorption breakthrough curves of simulated flue gas at the different flow rates. on 25 g **$Fe_5Co_5Mg_{10}CaO$** at 650 °C

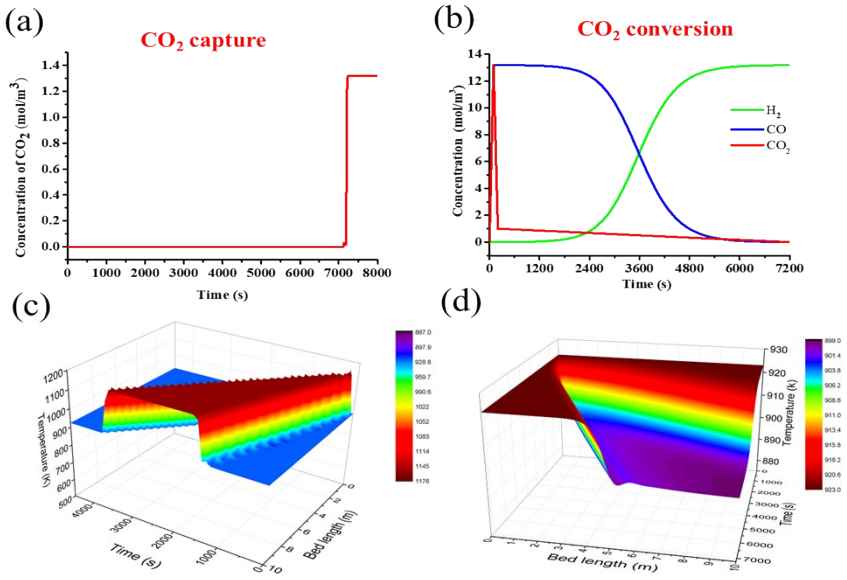


**Fig. S15.** Simulation profiles of the integrated $CO_2$ capture and conversion technology at the commercial scale (100,000 t/yr $CO_2$ emission) on 50 t **$Fe_5Co_5Mg_{10}CaO$** (a) the change of $CO_2$ concentration in the outlet with the time at the CaL adsorption stage, (b) the change of $CO_2$, CO, and $H_2$ concentrations with the time at the in-situ RGWR conversion stage. The temperature change profiles with time along the column at (c) the adsorption stage and (d) the conversion stage.

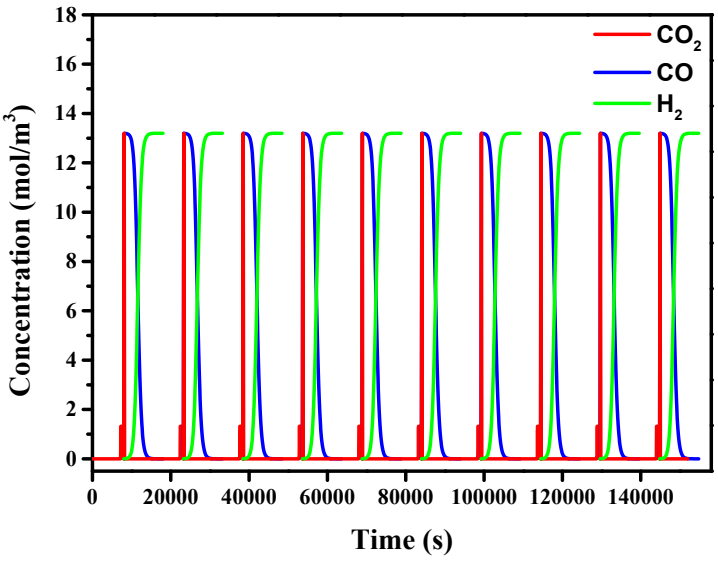


**Fig. S16** Stability simulation of 10 cycles of the integrated CaL/RWGS process at the commercial scale (100,000 t/yr $CO_2$ emission) at 650℃ on 50 t **$Fe_5Co_5Mg_{10}CaO$**.

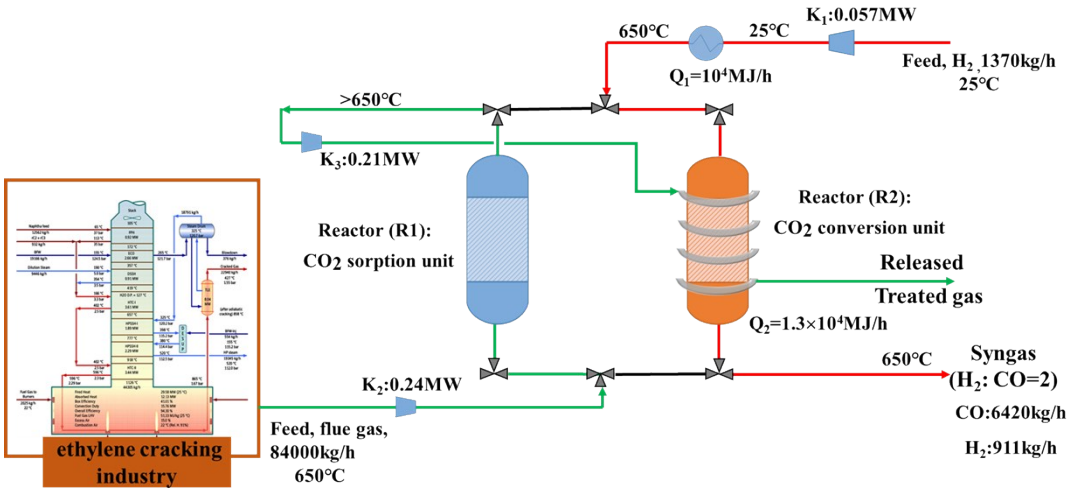


**Fig. S17** Schematic illustration of the integration of this $CO_2$ capture and in-situ conversion technology with a 100,000 t /yr ethylene plant, which works alternatively in the sequence of CaL capture and RWGS conversion in the manner of shifting between two columns.

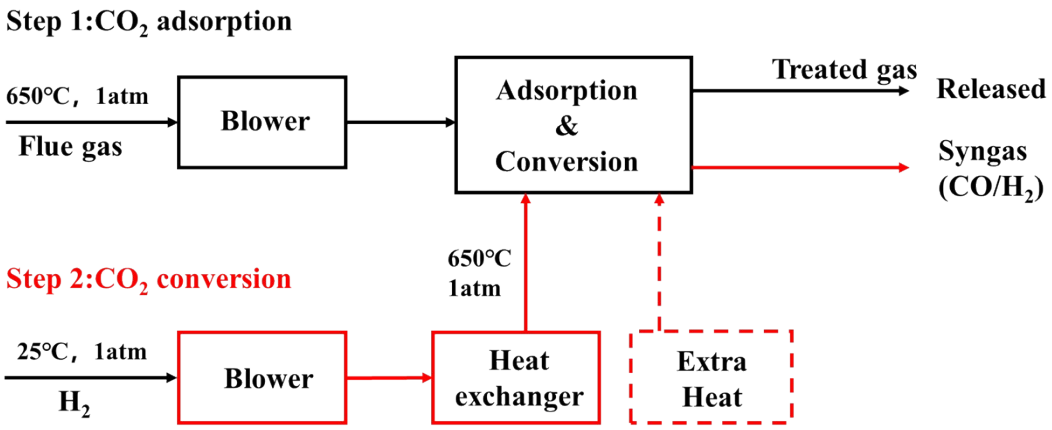


**Fig. S18** The main energy-consumption units during the integrated CaL/RWGS process.

**Table S1** Characteristic properties of elemental analysis, crystallite size and porosity of **$Fe_xCo_yMg_{10}CaO$.**

| Sample | weight ratio of Fe/Co | [a] Mass fraction ($W_t$. %) | | | [b] CaO (nm) | [c] $S_{BET}$ ($m^2\ g^{-1}$) | [d] $V_P$ ($cm^3\ g^{-1}$) |
|---|---|---|---|---|---|---|---|
| | | Fe | Co | Mg | | | |
| $Fe_{10}Mg_{10}CaO$ | Fe | 9.2 | n.a. | 9.3 | 38.4 | 21.4 | 0.079 |
| $Co_{10}Mg_{10}CaO$ | Co | n.a. | 9.3 | 9.4 | 33.6 | 17.8 | 0.068 |
| $Fe_5Co_5Mg_{10}CaO$ | 1 | 4.3 | 4.6 | 9.5 | 28.3 | 15.6 | 0.061 |
| $Fe_{6.7}Co_{3.3}Mg_{10}CaO$ | 2 | 5.8 | 2.7 | 8.8 | 32.1 | 16.7 | 0.070 |
| $Fe_{7.5}Co_{2.5}Mg_{10}CaO$ | 3 | 6.2 | 1.9 | 7.8 | 34.8 | 14.99 | 0.068 |
| $Fe_8Co_2Mg_{10}CaO$ | 4 | 7.2 | 1.2 | 8.5 | 30.8 | 13.39 | 0.063 |
| $Fe_{3.3}Co_{6.7}Mg_{10}CaO$ | 0.5 | 2.6 | 5.9 | 9.0 | 40.7 | 9.07 | 0.051 |

[a] measured by ICP

[b] average crystallite size calculated by $D_p = \frac{0.94\gamma}{\beta_{1/2}\cos\theta}$

[c] BET surface areas

[d] Total pore volume at a relative pressure ($P/P^0$) of 0.99

**Table S2.** Binding energies of $2p_{3/2}$ electrons of Co and Fe species in the fresh **$Fe_xCo_yMg_{10}CaO$.**

| Sample | $Co^{2+}$(eV) | $Co^{3+}$(eV) | $Fe^{2+}$(eV) | $Fe^{3+}$(eV) |
|---|---|---|---|---|
| $Fe_5Co_5Mg_{10}CaO$ | 781.9 | 780.8 | 710.6 | 713.2 |
| $Fe_{10}Mg_{10}CaO$ | / | / | 710.9 | 713.8 |
| $Co_{10}Mg_{10}CaO$ | 781.5 | 780.6 | / | / |

**Table S3.** Fitting parameters of the pseudo-second-order kinetic model for $CO_2$ capture on **$Fe_xCo_yMg_{10}CaO$** and CaO.

| Samples | Pseudo-second-order Kinetic equation | $k$ (g mmol$^{-1}$ min$^{-1}$) | $q_e$ (mmol g$^{-1}$) | $R^2$ |
|---|---|---|---|---|
| CaO | $t/q_t$ = 0.10699t+0.17669 | 0.0609 | 9.34 | 0.9967 |
| $Fe_{10}Mg_{10}CaO$ | $t/q_t$ = 0.1033t+0.2613 | 0.0415 | 9.68 | 0.9996 |
| $Co_{10}Mg_{10}CaO$ | $t/q_t$ = 0.09893t+0.46352 | 0.0211 | 10.11 | 0.9993 |
| $Fe_5Co_5Mg_{10}CaO$ | $t/q_t$ = 0.1006t+0.0929 | 0.1064 | 9.93 | 0.9995 |

**Table S4.** The comparison of $CO_2$ conversion performance with the state-of-the-art works.

| catalyst | Temperature (˚C) | $CO_2$ conversion (%) | CO selectivity (%) | Stability ($CO_2$ conversion) | References |
|---|---|---|---|---|---|
| $Fe_5Co_5Mg_{10}CaO$ | 650 | 90 | 100 | 10 cycles | this work |
| 10% Ni | 650 | 38 | 95 | 50 h | 11 |
| 10%Co | 600 | 38 | 100 | / | 12 |
| Ni/CeAl | 650 | 62 | 78 | / | 13 |
| Ni/CeAl | 750 | 68 | 95 | 45 h | 13 |
| $Ca_1Ni_{0.1}Ce_{0.033}$ | 650 | 51.8 | 100 | 20 cycles | 14 |
| Fe-Mo/$Al_2O_3$ | 600 | 36 | 35 | / | 15 |
| Co-Fe/$Al_2O_3$ | 650 | 50 | 48 | / | 16 |
| Fe-oxide | 600 | 31 | / | 19 h | 17 |
| magnetite | 600 | 21.3 | 85 | / | 17 |
| Fe/$Al_2O_3$ | 650 | 56 | 97 | 40 h | 18 |

**Table S5.** Binding energy of $2P_{1/2}$ and $2P_{3/2}$ electrons of the $Fe_5Co_5Mg_{10}CaO$ at different stages from high-resolution Fe 2p XPS spectra.

| Sample / Iron status | Fresh | After adsorption | After conversion |
|---|---|---|---|
| $Fe^{2+}$ | 710.6 eV | 710.3 eV | 710.2 eV |
| | 724.5 eV | 723.9 eV | 723.8 eV |
| $Fe^{3+}$ | 713.2 eV | 712.7 eV | 712.6 eV |
| | 727.3 eV | 726.3 eV | 726.2 eV |
| satellite | 718.6 eV | 718.4 eV | 718.2 eV |

**Table S6.** Binding energy of $2P_{1/2}$ and $2P_{3/2}$ electrons of the $Fe_5Co_5Mg_{10}CaO$ at different stages from high-resolution Co 2p XPS spectra.

| Sample / cobalt status | Fresh | After adsorption | After conversion |
|---|---|---|---|
| $Co^{2+}$ | 797.8 eV | 797.8 eV | 797.8 eV |
| | 781.9 eV | 781.5 eV | 781.5 eV |
| $Co^{3+}$ | 780.8 eV | 780.6 eV | 780.6 eV |
| | 795.8 eV | 795.8 eV | 795.8 eV |
| satellite | 786 eV | 786 eV | 786 eV |
| | 803 eV | 803 eV | 803 eV |

**Table S7.** The mass ratio changes of $Fe^{2+}/Fe^{3+}$ and $Co^{2+}/Co^{3+}$ in **$Fe_5Co_5Mg_{10}CaO$** at different stages calculated from high-resolution XPS spectra.

| **Sample** | **$Fe^{2+}$ / $Fe^{3+}$** | **$Co^{2+}$ / $Co^{3+}$** |
|---|---|---|
| Fresh | 0.47 | 1.62 |
| After adsorption | 0.54 | 1.6 |
| After conversion | 0.75 | 1.59 |

**Table S8.** The comparison between the microscale experiment and the scale-up experiment

| Parameters | | Microscale experiment | Scale-up experiment |
|---|---|---|---|
| Catalyst mass (g) | | 0.25 | 25 |
| Catalyst size (mesh/mm) | | 40-50/~0.4 | 10-20/~1.0 |
| Reactor geometry inside diameter (Φ mm) × height (mm) | | Φ 10 ×150 | Φ 25 ×500 |
| Flow rate (ml $min^{-1}$) | | 50 | 500 |
| Operation temperature ($^oC$) | | 650 | |
| Operation pressure (atm) | | 1 | |
| Adsorption | Breakthrough time (min) | 25 | 125 |
| | Total flue gas throughput (L) | 1.25 | 62.5 |
| | Total amount of $CO_2$ capture (L) | 0.05 | 5.10 |
| | Adsorption capacity (mmol $g^{-1}$) | 9.2 | 9.1 |
| Conversion | Time of conversion (min) | 30 | 90 |
| | CO yield (mmol $g^{-1}$) | 8.28 | 7.43 |
| | Carbon balance (%) | 100 | 95 |
| | $CO_2$ conversion (%) | 90 | 87 |
| | CO selectivity (%) | 100 | 100 |

**Table S9** the effect of flow rate on the performance of the scale-up integrated CaL/RWGS process at 650 ℃ on **$Fe_5Co_5Mg_{10}CaO$.**

| | **adsorption** | | | **Conversion** | | | | |
|---|---|---|---|---|---|---|---|---|
| **Flow rate (mL/min)** | Breakthrough time (min) | Total throughput (L) | $CO_2$ adsorption capacity (mmol g-1) | Time of conversion (min) | CO yield (mmol $g^{-1}$) | [a] Carbon balance (%) | $CO_2$ conversion (%) | CO selectivity (%) |
| 200 | 260 | 52 | 9.1 | 200 | 7.43 | 95 | 87 | 100 |
| 500 | 125 | 62.5 | 9.1 | 90 | 7.43 | 95 | 87 | 100 |
| 1000 | 25 | 25 | 9.0 | / | / | / | / | / |
| 2000 | 10 | 20 | 3.3 | / | / | / | / | / |

Note: /. Restricted by our experimental conditions and safety regulations, the conversion at the large flow rate of pure $H_2$ (>1000ml $min^{-1}$) was not tested.

**Table S10** Material flows (per hour) in each step during the integrated CaL/RGWR processes.

| Material | | Inlet gas | Adsorption (95%) | Conversion (85%) | Release | Product |
|---|---|---|---|---|---|---|
| $CO_2$ | (t/h) | 12.5 | 11.87 | 10.02 | 0.63 | 1.85 |
| | (kmol/h) | 284 | 269.8 | 229.3 | 14.2 | 40.5 |
| $N_2$ | (t/h) | 71.5 | 0 | 0 | 71.5 | 0 |
| | (kmol/h) | 2556 | | | 2556 | |
| $H_2$ | (t/h) | 1.37 | 0 | 0.459 | 0 | 0.911 |
| | (kmol/h) | 687.9 | | 229.3 | | 455.5 |
| CO | (t/h) | 0 | 0 | 6.42 | 0 | 6.42 |
| | (kmol/h) | | | 229.3 | | 229.3 |
| $H_2O$ | (t/h) | 0 | 0 | 4.13 | | 4.13 |
| | (kmol/h) | | | 229.3 | | 229.3 |
| Electricity for gas transport (kWh) | | 507 [a] | | | | |
| Electricity for heating (kWh) | | | | 1912 | | |
| Natural gas for heating $H_2$ ($m^3$/h) | | 376 | | | | |

Note: a, the electricity for gas transport including flue gas (240 kWh), H2 (57 kWh) and treated gas released (210 kWh)

**Table S11** the price and consumption of each material per year (Assuming the yearly operating time is 8000 h/yr)

| Item | Price[a] | Consumption ( /yr) |
|---|---|---|
| $H_2$ | 1400 \$/t | 8960 t [b] |
| $CO_2$ tax | 7 \$/t | 100000 t |
| Syngas | 170 \$/t | 58648 t |
| $Fe_5Co_5Mg_{10}CaO$ | 3500 \$/t | 167 t [c] |
| Natural gas for heating $H_2$[d] | 0.43 \$/$m^3$(STP) | $4\times10^6$ $m^3$ |
| Blower (electricity) | | $4.05\times10^6$ KWh |
| Extra heat for RWGS (electricity) | | $1.53\times10^7$ KWh |
| Total electricity \$/kWh | 0.12 \$/kWh | $1.8\times10^7$ kWh [e] |

Notes:

a, the price is according to the market of China.

b, the total amount of $H_2$ consumption is 10,960 t/y, including 2,000 t/yr by-product of $H_2$ in the 100,000 t/yr ethylene plant.

c, the amount of $Fe_5Co_5Mg_{10}CaO$ in one column is 50 t, the cycle stability is set as 100 days, i.e. the consumption of $Fe_5Co_5Mg_{10}CaO$ is 0.5 t/d.

d, heating $H_2$ by burning nature gas.

e, the total electricity consists of two parts (the blowers and the extra heating for RWGS).

## References


1. Y. Ho and G. Mckay, *Process Biochem.*, 1999, **34**, 451-465.

2. Turton, R., Bailie, R.C., Whiting, W.B., Shaeiwitz, J.A., Bhattacharyya, D., 2012. Analysis, Synthesis, and Design of Chemical Processes, 4th ed. Prentice Hall

3. J. Baltrusaitis and W. L. Luyben, *ACS Sustainable Chem. Eng.*, 2015, **3**, 2100-2111.

4. P. R. Kumar, H. B. Yahia, I. Belharouak, M. T. Sougrati, S. Passerini, R. Amin and R. Essehli, J. Solid State Electrochem., 2019, 24, 17-24.. Baltrusaitis and W. L. Luyben, *ACS Sustainable Chem. Eng.*, 2015, **3**, 2100-2111.

5. D.-Y. Lee and A. Elgowainy, Int. J. Greenh. Gas Control, 2018, 43, 20143-20160.\

6. E. Rezaei and S. Dzuryk, Chem. Eng. Res. Des., 2019, 144, 354-369.

7. J. Baltrusaitis and W. L. Luyben, ACS Sustainable Chem. Eng., 2015, 3, 2100-2111.

8. X. Luo, M. Wang, E. Oko and C. Okezue, Appl. Energy, 2014, 132, 610-620.5. L.Wang,H.Liu, Y. Chen and S. Yang, *Int. J. Hydrogen Energy*, 2017, **42**, 3682-3689.

11. A. Ranjbar, A. Irankhah and S. F. Aghamiri, *Journal of Environmental Chemical Engineering*, 2018, **6**, 4945-4952.

12. L. Wang, H. Liu, Y. Chen and S. Yang, *Int. J. Hydrogen Energy*, 2017, **42**, 3682-3689.

13. L. Yang, L. Pastor-Pérez, S. Gu, A. Sepúlveda-Escribano and T. Reina, *Applied Catalysis B: Environmental*, 2018, **232**, 464-471.

14. H. Sun, J. Wang, J. Zhao, B. Shen, J. Shi, J. Huang and C. Wu, *Appl. Catal., B*, 2019, **244**, 63-75.

15. A. G. Kharaji, A. Shariati and M. Ostadi, *Journal of nanoscience and nanotechnology*, 2014, **14**, 6841-6847.

16. S. Sengupta, A. Jha, P. Shende, R. Maskara and A. K. Das, *Journal of Environmental Chemical Engineering*, 2019, **7**.

17. D. H. Kim, S. W. Han, H. S. Yoon and Y. D. Kim, *J. Ind. Eng. Chem.*, 2015, **23**, 67-71.

18. L. Pastor-Pérez, M. Shah, E. le Saché and T. Ramirez Reina, *Catalysts*, 2018, **8**, 608.